1-1-2015

Effects of grain boundaries in oxide scale on tribological properties of nanoparticles lubrication

Xianglong Yu
University of Wollongong, xly991@uowmail.edu.au

Zhengyi Jiang
University of Wollongong, jiang@uow.edu.au

Jingwei Zhao
University of Wollongong, jzhao@uow.edu.au

Dongbin Wei
University of Wollongong, dwei@uow.edu.au

Cunlong Zhou
Taiyuan University of Science and Technology, zcunlong@163.com

See next page for additional authors

Effects of grain boundaries in oxide scale on tribological properties of nanoparticles lubrication

Abstract

The characters of grain boundaries in oxide layers formed on substrates influence adhesion and friction behaviour, surface fracture and wear during high temperature steel processing. In this work, an electron backscattered diffraction (EBSD) analysis was conducted to investigate the role of surface grain boundary and orientation in magnetite (Fe_3O_4)/haematite (α-Fe_2O_3) scale during hot rolling, and further evaluate their effects on tribological properties of water-based nanoparticles lubrication. The results demonstrate that Fe_3O_4 (100) plane is strongly sensitive to the surface characteristics as the minimisation of surface energy. Coincident site lattice (CSL) boundaries in microstructure is in presence of $\Sigma 3$ in the Fe_3O_4 and $\Sigma 13b$ in the Fe_2O_3 of the substrates subjected to a thickness reduction of 28% and cooling rate of 28 ° C/s. This is due in great part to the changes in crystal slip systems. These low-Σ CSL boundaries in oxide scale offer obstacles to the propagation of cracks, where some of nanoparticles collected would be trapped at the interface and thereby may cause high wear rates. A lubrication mechanism is proposed to explain the grain boundary effect on nanoparticles lubrication, and further to determine the dependence of frictional behaviour on surface energy, crystallographic preferred orientation (microtexture) and crystal structure. These results provide an intriguing new insight into the application of water-based lubricant with graphite nanoparticles.

Keywords

grain, boundaries, oxide, effects, scale, tribological, lubrication, nanoparticles, properties

Disciplines

Engineering | Science and Technology Studies

Publication Details

Yu, X., Jiang, Z., Zhao, J., Wei, D., Zhou, C. & Huang, Q. (2015). Effects of grain boundaries in oxide scale on tribological properties of nanoparticles lubrication. Wear, 332-333 1286-1292.

Authors

Xianglong Yu, Zhengyi Jiang, Jingwei Zhao, Dongbin Wei, Cunlong Zhou, and Qingxue Huang

Effects of grain boundaries in oxide scale on tribological properties of nanoparticles lubrication

Xianglong Yu [a], Zhengyi Jiang [a*], Jingwei Zhao [a], Dongbin Wei [a, b], Cunlong Zhou [c*], Qingxue Huang [c]

[a] School of Mechanical, Materials and Mechatronic Engineering, University of Wollongong, Wollongong, NSW 2522, Australia.

[b] School of Electrical, Mechanical and Mechatronic Systems, University of Technology, Sydney, NSW 2007, Australia.

[c] Shanxi Provincial Key Laboratory on Metallurgical Device Design and Theory, Taiyuan University of Science and Technology, Shanxi 030024, China.

Abstract

The characters of grain boundaries in oxide layers formed on substrates influence adhesion and friction behaviour, surface fracture and wear during high temperature steel processing. In this work, an electron backscattered diffraction (EBSD) analysis was conducted to investigate the role of surface grain boundary and orientation in magnetite (Fe_3O_4) / hematite (α-Fe_2O_3) scale during hot rolling, and further evaluate their effects on tribological properties of water-based nanoparticles lubrication. The results demonstrate that Fe_3O_4 (100) plane is strongly sensitive to the surface characteristics as the minimisation of surface energy. Coincident site lattice (CSL) boundaries in microstructure is in presence of $\Sigma 3$ in the Fe_3O_4 and $\Sigma 13b$ in the Fe_2O_3 of the substrates subjected to a thickness reduction of 28% and cooling rate of 28 °C/s. This is due in great part to the changes in crystal slip systems. These low-Σ CSL boundaries in oxide scale offer obstacles to the propagation of cracks, where some of nanoparticles collected would be trapped at the interface and thereby may cause high wear rates. A lubrication mechanism is proposed to explain the grain boundary effect on nanoparticles lubrication, and further to determine the dependence of frictional behaviour on surface energy, crystallographic preferred orientation (microtexture) and crystal structure. These

results provide an intriguing new insight into the application of water-based lubricant with graphite nanoparticles.

Keywords: Oxide scale; Magnetite; Hematite; Nanoparticles lubrication; Tribological properties; Electron backscattered diffraction.

*Corresponding authors: Tel: 61 2 42214545; Fax: 61 2 42215474; Email: jiang@uow.edu.au (Z. Jiang). Tel: 86 18635592059; Fax: 86 351 6963332; Email: zcunlong@163.com (C. Zhou).

1. **Introduction**

Water-based nanoparticles lubricants have recently emerged as environmentally friendly and energy saving alternative to conventional oil-based lubricants for metal processing at high temperatures [1, 2]. Since most metals and alloys inevitably grow surface oxide layers due to thermal oxidation at elevated temperatures [3–5], graphite in oxidising environments becomes the spotlight in the nanoparticle additives for lubrication in hot rolling [6]. In some cases, the environment can dominate surface characteristics of two solids in contact during nanoparticle lubrication [7, 8]. Correspondingly, many different surface properties of metals and alloys will influence tribological performance [9, 10]. These surface properties include surface energy, crystallographic orientation, grain boundaries, texturing of surface and crystal structure [11, 12]. Therefore, it is widely expected that tailoring the atomic structure of the grain boundary can be possible to enhance tribological properties during nanoparticles lubrication, and further improve surface quality of steels [13, 14]. However, characterisation of texture evolution and grain boundaries in deformed oxide layers has remained less investigation.

Texture in material science is defined, more concisely, as crystallographic preferred orientation, i.e. the tendency how the atomic planes in a volume of crystal are positioned relative to a fixed reference [15, 16]. This is different from texturing of the surface in the field of tribology [6, 17, 18] or the road and traffic engineering [19], which is defined as the repetitive or random deviation from the nominal surface that forms the three-dimensional topography of the surface, and represented by roughness, waviness, lay and flaws [1, 20]. Generally, an approach, such as electron backscattered diffraction (EBSD), that deals with the orientation statistics of a population of individual grains and their spatial location, i.e. the orientation topography, has been termed as microtexture – the conjoining of microstructure and texture [15, 21]. To avoid ambiguity, a texture that reflects an

average value obtained from many different grains is often called macrotexture [15, 22], which is obtained from the x-ray or neutron diffraction.

In addition to crystallographic orientation, the presence of grain boundaries in the oxide layers influences adhesion and friction behaviour, surface fracture and wear [1, 13]. A grain boundary is a strained condition in that many dislocations present to help accommodate the misfit or mismatch in adjacent orientations. These high energy regions at the surface could make sliding more difficult and increase the friction force of materials [13, 23]. Nevertheless, different crystallographic directions will have different mechanical properties. As such, the orientation of a crystallographic slip plane will change when a counterpart moves out from a grain across a boundary to another grain. This could also be associated with change in friction [1]. Thus, the grain boundary can contribute to the overall surface energy and the corresponding tribological behaviour. Generally, it is widely believed that coincident site lattice (CSL) boundaries have both lower grain boundaries energy and higher migration mobility than other general boundaries [24, 25]. The low-energy CSL boundaries can be used to improve the crack or oxidation resistance of the materials [25, 26]. However, detailed information on what kinds of CSL boundaries have beneficial properties and how the typical processing routes actually produce high fractions of CSL boundaries is still lacking. Furthermore, grain boundary engineering (GBE) is largely confined at present to face centre cubic (fcc) metallic systems, such as stainless steel [27, 28], nickel alloys [29, 30] and aluminium alloys [31]. Little is currently known concerning grain boundary characters of cubic magnetite (Fe_3O_4) and hexagonal hematite (α-Fe_2O_3).

Analysis of the microtexture in oxide phases and their orientation relationship (OR) is generally conducted via EBSD [32–38]. Cubic Fe_3O_4 and wustite ($Fe_{1-x}O$, 1-x=0.83–0.95) share a strong <100> texture and a cube-cube OR in undeformed oxide scale formed on whatever the steel substrate [16, 32]. In contrast, the deformed $Fe_{1-x}O$ develops a pronounced <100> fibre component

using plane strain compression [33, 36]. In view of texture analysis of iron oxides in the geography field [37, 38], ambiguities remain what kind of microtexture in deformed Fe_3O_4 and α-Fe_2O_3 will be developed during hot rolling, and what its evolution will be. Also, few work on the grain boundary effect leads to the change of tribological properties with the polycrystalline tungsten or copper [1, 13, 25], but often uncorrelated.

To examine the grain boundary effect, the present study aims to detect the grain orientations of the steel substrate and oxide layers after hot rolling-accelerated cooling (HR-AC) process, and then to find how the effect is acting on. Specifically, an EBSD texture-based analysis is first conducted to investigate the microtexture and misorientation characteristics of Fe_3O_4 and α-Fe_2O_3 in the tertiary oxide scale after HR-AC tests. These grain boundary characters and texture evolution are then used to determine the dependence of frictional behaviour on crossing grain boundaries based on the slip behaviour of cubic Fe_3O_4 and hexagonal α-Fe_2O_3. Finally, an attempt is made to simulate the formation and propagation of cracks along the Fe_3O_4 grain boundaries and thereby to provide a further understanding on tribological properties of nanoparticles lubrication.

2. Experimental and analytical procedures

2.1 Material and HR-AC test

The material used was a Nb-V-Ti microalloyed low carbon steel for automobile beam. Its chemical compositions are listed in Table 1. Flat steel sheets (400 × 100 × 3 mm^3) with an average surface roughness of about 0.5 μm were hot rolled on a 2-high Hille 100 experimental mill combined with an accelerated cooling system. Full details of the experimental instruments can be found elsewhere [39, 40]. The following procedure was conducted for every HR-AC test. Each sample was reheated to 900 °C at a rate of 1.7 °C/s under a high purity inert gas atmosphere, and held for 15 min to

ensure a uniform temperature and homogenise the austenite grains. The reheated sample was then given a single rolling thickness reduction (TR, 10%–28%) at a rolling speed of 0.3 m/s without any lubrication followed by an accelerated cooling with the cooling rates (CRs) of 10–28 °C/s. Finally, the HR-AC samples were air cooled to obtain the tertiary oxide scale [4] at room temperature. This presumes, of course, the grown oxide layers are subject to the same deformation ratios as the corresponding hot-rolled steel substrate. In this case, the heat treatment during hot rolling aims to obtain the large initial grain size in oxide scale. The polycrystalline matrix of oxide layers was used to determine the influence of crossing grain boundaries on slip behaviour.

Table 1 Chemical compositions of the microalloyed low carbon steel.

Elements	C	Si	Mn	P	Cr	S	Al	N	Nb +V+ Ti	Fe
wt.%	0.1	0.15	1.61	0.014	0.21	0.002	0.034	0.003	0.016-0.041	Bal.

2.2 Analytical methodology

Oxidised samples for subsequent examination with electron microscopes were cut from the centre of the hot-rolled sheet along the plane of the rolling direction (RD) and normal direction (ND). After gold deposition, the edges for cross sectional analysis were ground by SiC papers with 2000 mesh, and then ion-milled at 6 kV for 5 h using a TIC020 system. Microstructure characterisation was studied using a JEOL JSM 7001F Schottky field emission gun (FEG) scanning electron microscope (SEM) with a Nordlys-II (S) EBSD detector, operated at an acceleration voltage of 15 kV, a probe current of around 2–5 nA, a working distance of 15 mm, and a step size of 0.125 μm. In addition to atomic configuration, Lammps simulator was applied to study the growth of crack tips in oxide layers, whereas Material studio 5 software package was used to evaluate the tribological properties at the interface during nanoparticle lubrication.

2.3 Grain reconstruction

Post-processing of acquired dataset was carried out using Channel 5 software, where both misorientation and microtexture data were extracted from the EBSD maps. First for orientation noise reduction, an angular resolution for the grain reconstruction was maintained at a constant value of 2°. Consequently, $2° \leq \theta < 15°$ misorientations are defined as low-angle grain boundaries (LAGBs), whereas, the high-angle grain boundaries (HAGBs) are $\theta \geq 15°$. Secondly, phase identification is based on the structural data related to the crystal symmetry and lattice parameters of the suspected phases. In case of the oxide scale, each phase has a different space group (α-Fe, *Imm*; $Fe_{1-x}O$, *Fmm*; Fe_3O_4, *Fdm*; α-Fe_2O_3, *Rc*), and different lattice parameters. α-Fe, $Fe_{1-x}O$ and Fe_3O_4 in cubic symmetry with lattice parameters (*a*) of 0.287 nm, 0.431 nm, and 0.840 nm respectively, and α-Fe_2O_3 in a trigonal structure with *a*=0.504 nm and *b*=1.377 nm [32, 33, 36–38]. The EBSD phase maps were finally divided into three subsets comprising α-Fe, Fe_3O_4 and α-Fe_2O_3 for microtexture based analysis. Orientation distributions of the three subsets were calculated from the data on individual grain orientations collected. The grain orientation $g = (\phi_1, \Phi, \phi_2)$ is expressed by the three Euler angles in Bunge notation [15, 22]. As such, a grain boundary can be classified geometrically in terms of the relative misorientation between the neighboured grains. This relative misorientation can be defined by misorientation axis and angle, with certain specific combinations resulting in a CSL. The degree of coincidence is represented by the reciprocal density of common lattice points, denoted as the Σ number. In this case, CSL boundaries can be identified based on Brandon's criterion [41]. It is generally believed that CSL boundaries with low Σ orientation ($\Sigma \leq 49$) display improved physical and chemical properties relative to general or high CSL boundaries ($\Sigma > 49$).

3. Results and discussion

3.1 Microstructure characterisation

EBSD inverse pole figure (IPF) orientation maps shown in Fig. 1 indicate the microstructural evolution with progressively greater TRs and CRs after HR-AC experiments. Grains with the colour coded displayed their orientations is related to a stereographical triangle, where Fig. 1d is for the cubic symmetry material such as $Fe_{1-x}O$, Fe_3O_4 and α-Fe, and Fig. 1e is for the hexagonal α-Fe_2O_3. The grain size of granular Fe_3O_4 was determined as 3 μm in the outer layer of oxide scale at a TR of 28% and a CR of 28 °C/s (Fig. 1c). Details of the grain size associated with the steel substrate can be found in our previous study [42]. The intermediate Fe_3O_4 layer on the IPF maps in Fig. 1 holds a columnar-shape microstructure between the outer granular grains and the Fe_3O_4 seam. This is due in great part to the retained $Fe_{1-x}O$ during the lateral grain growth at high temperature [34, 35]. Most of the Fe_3O_4 grains have a preferred orientation with <001> parallel to the ND, i.e. along the oxide growth direction, as the increase of the TRs and CRs. The grain growth of Fe_3O_4 with <001>//ND texture may be determined by the minimisation of surface energy (SE), where the SE of the crystallographic planes of Fe_3O_4 are: SE(100)=1.5, SE(110)= 1.8 and SE(111)=2.2 J m^{-2} parallel to the oxide growth [32, 43]. Nevertheless, the lack of this sharp texture in Fe_3O_4 of the sample at the lower TR and CR (10%, 10 °C/s in Fig. 1a) suggests that the rolling process and subsequent cooling affect the texture and grain size of the formed oxide scale.

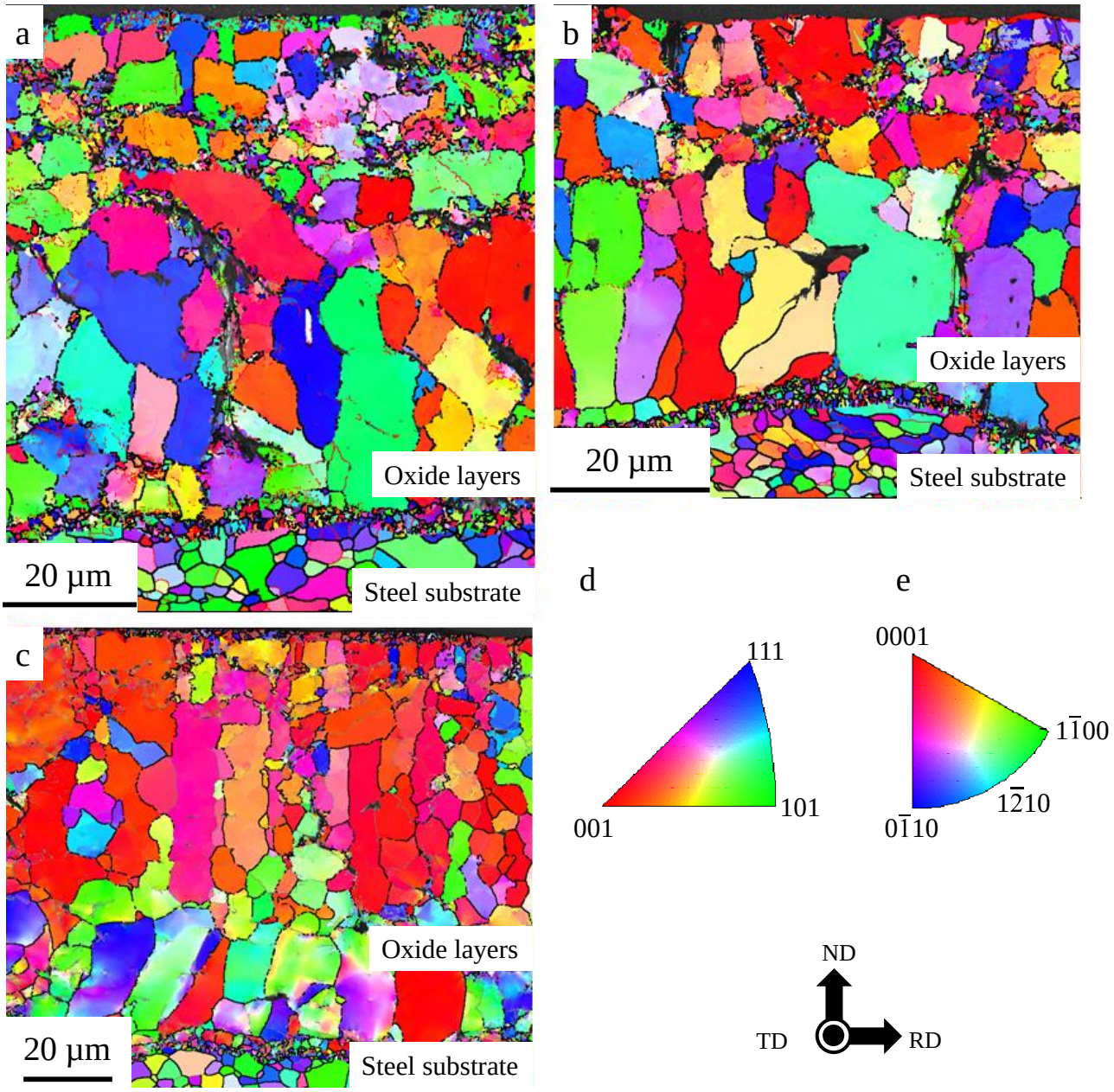

Fig. 1 EBSD IPF orientation maps of the samples at the TRs and CRs of (a) 10%, 10 °C/s, (b) 13%, 23 °C/s, (c) 28%, 28 °C/s, a colour key for the (d) cubic symmetry of α-Fe, $Fe_{1-x}O$ and Fe_3O_4, and (e) hexagonal α-Fe_2O_3.

3.2 Microtexture development of oxide scale

Microtexture analysis has been investigated to verify the microstructural evolution of deformed oxide layers and steel during hot rolling. Fig. 2 shows the pole figure (PF) of Fe_3O_4 in the oxide layers formed on the hot-rolled steel with a TR of 10% and a CR of 10 °C/s. A strong {100} and a

weak {110} fibres texture component develops in the oxidised surface of steel substrate. This texture development will contribute to the easy gliding in hexagonal graphite during lubrication and thereby to decrease the coefficient of friction. This is because the direction of easy slip in graphite is related to the orientation relationship between graphite and surface oxide [32, 44–46], (111) Fe_3O_4 parallel to (0001) graphite. The {0001} plane is crystallographic plane having close packed oxygen anions, thus deformation occurs across close packed oxygen planes [32, 46]. This is the reason why the basal plane {0001} will be aligned parallel to the crystallographic plane in Fe_3O_4 where graphite undergoes deformations. This result provides a strong insight into the application of water-based lubricant with graphite nanoparticles.

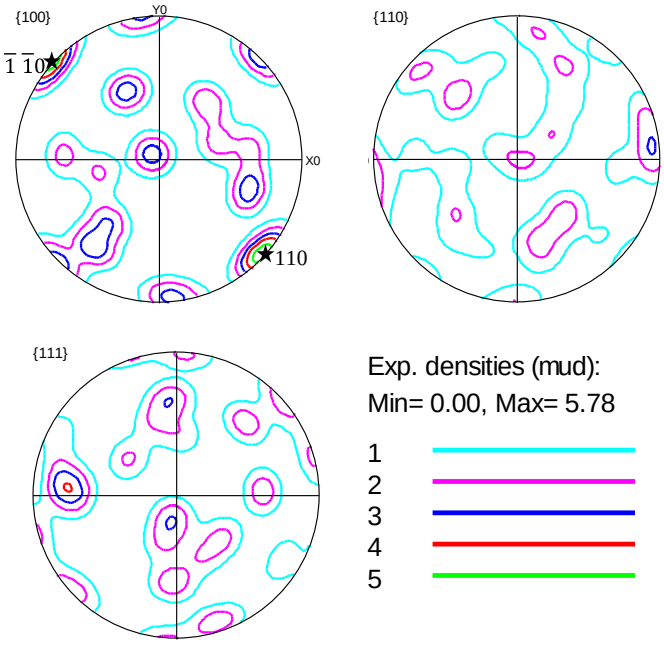

Fig. 2 Pole figures (PF) of Fe_3O_4 in oxide scale formed on the surface of the hot-rolled sample with a TR of 10% and a CR of 10 °C/s.

3.3 Grain boundary character distribution

The fractions of grain boundaries classified as HAGBs, LAGBs and CSL boundaries are shown in Figs. 3 and 4 for Fe_3O_4 and α-Fe_2O_3 of the samples with different TRs and CRs. The distribution of

misorientation angles in cubic Fe_3O_4 has a second largest peak at 60° and a cutoff at 62.8° (Fig. 3c), whereas hexagonal α-Fe_2O_3 has obvious peaks at 30°, 60°, 85° and a cutoff at 95° (Fig. 3d). The misorientation axis-angle distribution was calculated to determine the relevant misorientation axes at each of the peaks in Fig. 3c and d, and thereby to give a high proportion of CSL boundaries. The peaks in the 57–63° section (Fig. 3a) correspond to 60°/<111> (Σ3) misorientation marked in Fig. 3c. Misorientation peaks occur in α-Fe_2O_3 (Fig. 3b) for axes near <0001> in the angle range of 27–63°, and <102> in the angle range of 63–83°. For α-Fe_2O_3 the relatively high densities correspond to 57.42°/<110> (Σ13b) and 84.78°/<010> (Σ19c) [47]. Furthermore, CSL boundaries distributions in Fig. 4 reveal that Fe_3O_4 carries a high proportion of Σ3, Σ5 and Σ7, whereas α-Fe_2O_3 has a profound fraction of Σ7, Σ13b and Σ19c. In is noted that coherent twins have been excluded from this analysis, which results in a significantly lower fraction of Σ3 boundaries. In any case, it becomes clear that these low CSL grain boundary characteristics in Fe_3O_4 and α-Fe_2O_3 can be used to enhance crack resistance and further improve tribological properties of oxidised steels during hot rolling.

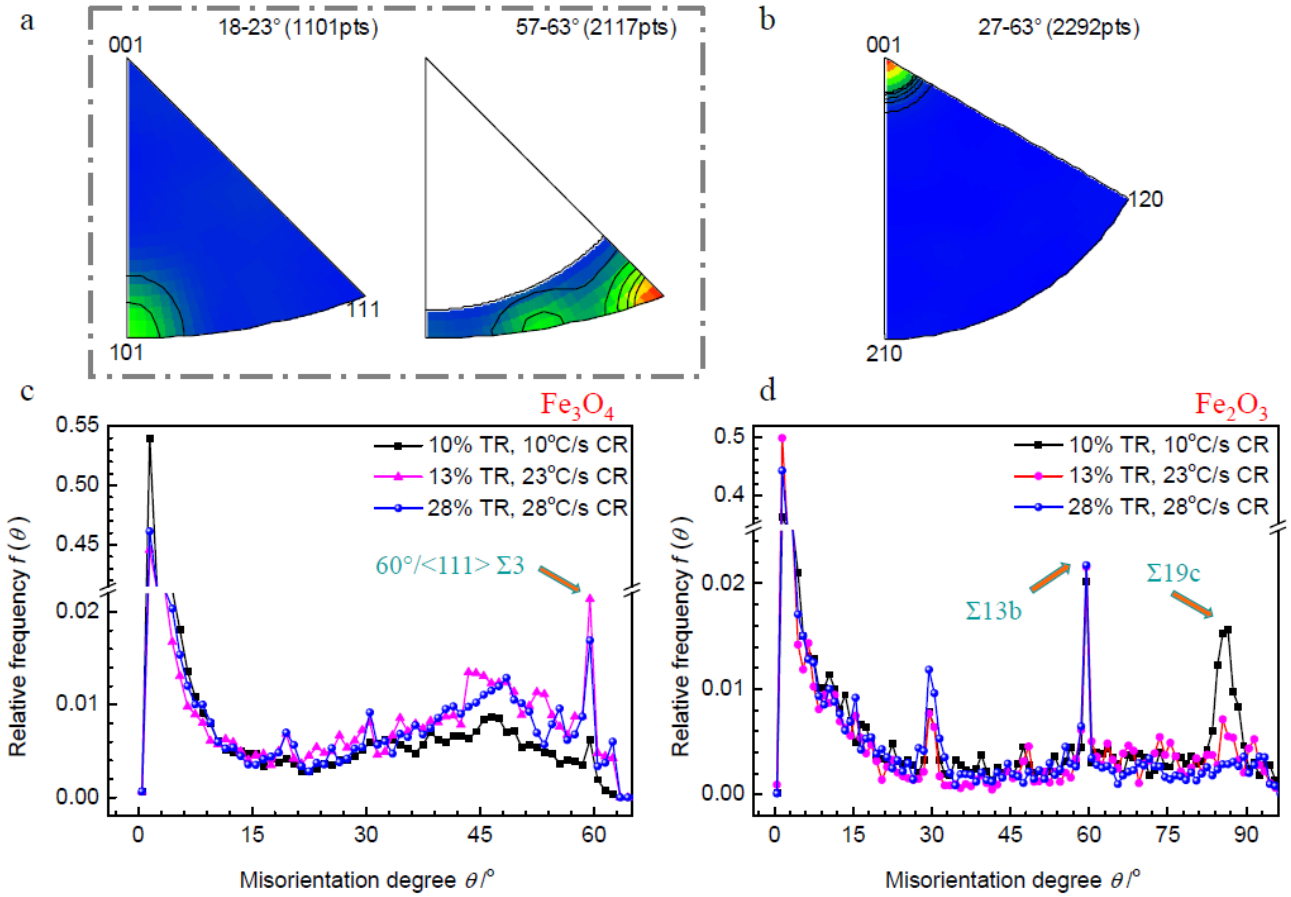

Fig. 3 Distributions of misorientation axes for grain boundaries in (a) Fe_3O_4, (b) α-Fe_2O_3, of the sample with a TR of 10% and a CR of 10 °C/s; distribution of grain boundary misorientation angels (c) from 2 to 62.8° for cubic Fe_3O_4, and (d) to 95° for hexagonal α-Fe_2O_3, of the samples with different TRs and CRs. Note the break in the vertical axis to emphasise the smaller peaks in comparison to the dominant peak less than 15°.

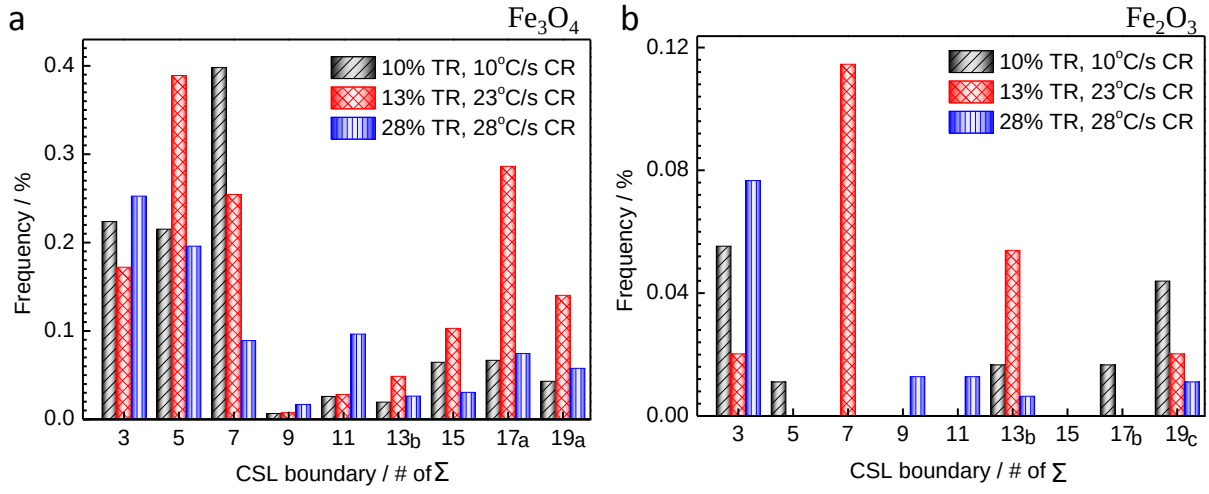

Fig. 4 Histogram plots of CSL boundary distribution for (a) Fe_3O_4 and (b) α-Fe_2O_3, of the samples with different TRs and CRs.

3.4 Variation of tribological properties in grain boundaries

The friction characteristics with oxide scale also reveal a grain boundary effect – a profound dependence of friction on crystallographic direction and orientation, and grain boundary characters. Fig. 5 plots the coefficient of friction and rolling force as a function of different TRs, corresponding to microtexture and CSL boundaries of Fe_3O_4 and α-Fe_2O_3 at the top of the figure. In the case of hot rolling, the coefficient of friction was calculated by forward slip, and similar method can be found elsewhere [48]. The Orowan equation solved according to Alexander [49] was used to determine the rolling force. As seen in Fig. 5, an increase in rolling force is accompanied by a decrease in coefficient of friction. Fe_3O_4 subjected various TRs develops strong 100 fibres. Moreover, variation of direction on this particular plane leads to a significant influence on friction. Moving from the <110> (10% TR) to the <100> (13% TR) direction, the coefficient of friction decreases from 0.101 to 0.068. This is due in great part to the changes in crystal slip systems in moving out of a grain, across the grain boundary and into another grain. This result is further confirmed by the presence of CSL boundaries Σ3 in the Fe_3O_4 at a high TR of 28%. It infers that coherent twins could enhance the migration of grain boundaries, thereby the coefficient of friction decreases. In case of α-Fe_2O_3 with a strong preferential crystallographic orientation in the normal direction of the (0001) basal plane, the microtexture strength is thought to be driven by the low surface energy (1.52J m^{-2}) of the (0001) plane of α-Fe_2O_3 [50]. A strong {0001}<100> texture component developed with CSL boundaries from Σ19c (10% TR) to Σ13b (13%–28% TRs) is a direct consequence of the favoured basal plane slip.

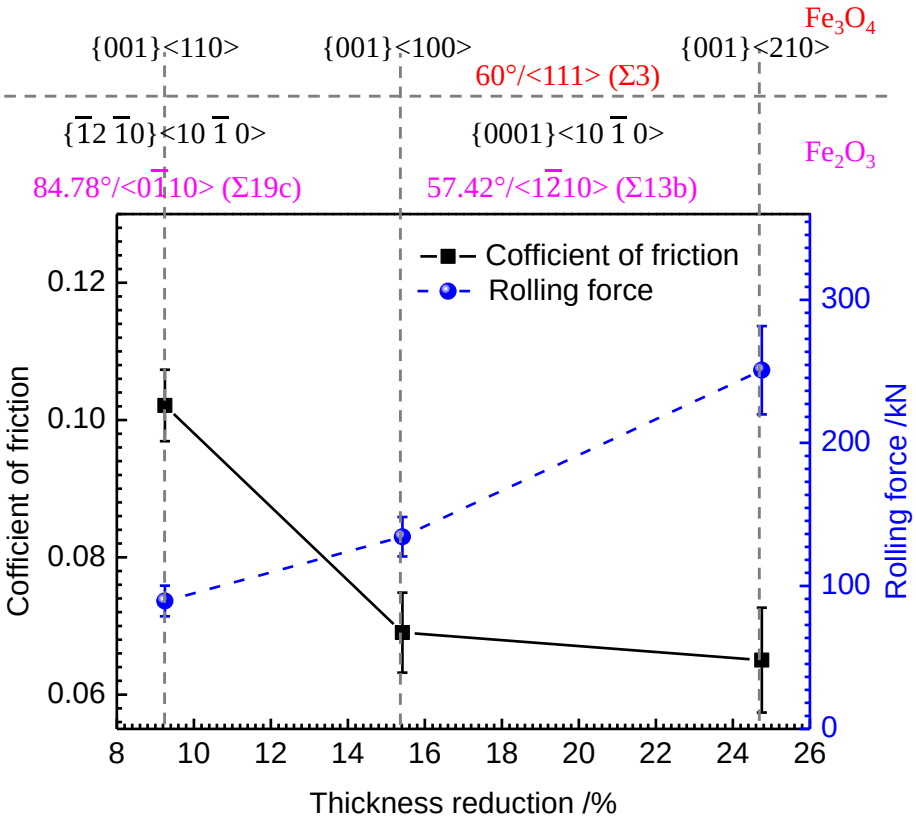

Fig. 5 The variation of the coefficient of friction and rolling force in different thickness reductions, microtexture and grain boundary characters in Fe_3O_4/Fe_2O_3 scale during hot rolling.

3.5 Crack initiation in nanoparticles lubrication

The formation and propagation of cracks along the Fe_3O_4 grain boundaries create paths for nanoparticles easy penetration. Some of these nanoparticles would be trapped at the interface and may cause high wear rates. Fig. 6 indicates atomic configurations of nanoparticles flow along interface of tip of brittle crack. A stress-dependent chemical reaction between water vapour and the interface would make the understanding of tribological properties elusive. The stress is the greatest at the tips of small cracks in the material, and consequently the reaction proceeds at its greatest rate from these tips [51]. However, it is believed that low-angle and low-ΣCSL boundaries in microstructure offer obstacles to the propagation of cracks as they minimise the solute effects and reduce the interaction between the interfaces and glissile dislocation [52]. In this case, the oxide scale is easy to crack in presence of Σ13b and Σ19c in α-Fe_2O_3 compared to Fe_3O_4 with Σ3 (Fig. 3c).

Thus, it is possible that during this time, tailoring specific grain boundaries can provide new insight into means of suppressing propagation of cracks when it is undesirable and into means of producing specific trapped nanoparticles when it is desired. In our experiments, some of these processes, such as a desired TR (>28%) can reduce cracks along the Fe_3O_4 grain boundaries, are underway to manipulate tribological properties of nanoparticles lubrication.

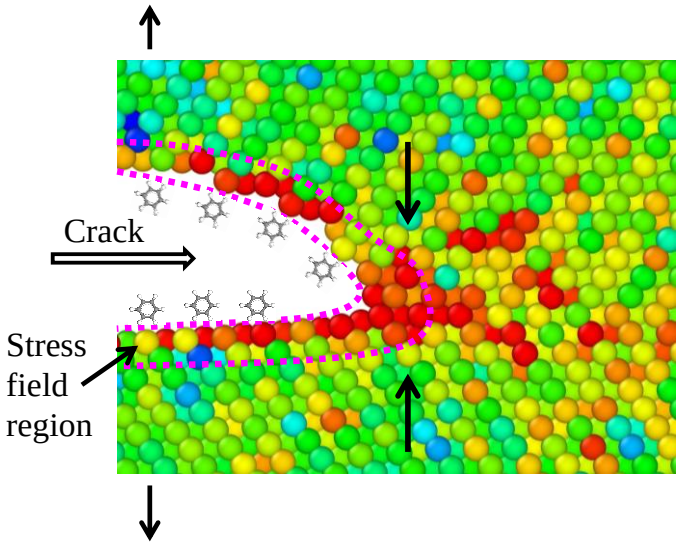

Fig. 6 Atomic configurations of nanoparticles flow along interface of tip of brittle crack. Note the size proportion of nanoparticles near the crack wall to emphasise the dominant crack tip.

4. Conclusions

In this present study, the grain orientations and boundary characters in Fe_3O_4/α-Fe_2O_3 scale form on a Nb-V-Ti steel subjected to the TRs of 10%–28% and CRs of 10–28 °C/s have been quantitatively characterised and systematically analysed. The following conclusions can be drawn.

(1) In the tertiary oxide scale, the Fe_3O_4 grains have the preferred orientation with <001> parallel to the oxide growth direction. This is a direct consequence of the minimisation of surface energy on the (100) Fe_3O_4 crystallographic planes.

(2) The deformed oxide layers comprise a high proportion of LAGBs and low CSL boundaries. Fe_3O_4 on the samples at a TR of 10% and CR of 10 °C/s develops 60°/<111> (Σ3), and α-Fe_2O_3 for 57.42°/<110> (Σ13b) and 84.78°/<010> (Σ19c). These low CSL grain boundaries would be expected to enhance crack resistance and further improve tribological properties of nanoparticle lubrication during hot rolling.

(3) The coefficient of friction decreases when the moving from the <110> (10% TR) to the <100> (13% TR) direction on the (100) Fe_3O_4 crystallographic planes. This is due in great part to the changes in crystal slip systems. The presence of CSL boundaries Σ3 in the Fe_3O_4 at a high TR of 28% confirms that low CSL boundaries could enhance the migration of grain boundaries thereby to reduce the friction. A similar effect occurs on {0001} Fe_2O_3 plane with CSL boundaries from Σ19c (10% TR) to Σ13b (13%–28% TRs), which can be attributed to the favoured basal plane slip.

(4) A lubrication mechanism presented here reveals that the propagation of cracks along the Fe_3O_4 grain boundaries could create a dish to collected nanoparticles during lubrication, and thereby resulting in high wear rates. As such, it is possible that low-angle and low-ΣCSL boundaries in microstructure offer obstacles to the propagation of cracks and further to decrease friction and wear. The better understanding we have gained could aid in the choice and design of the desired tribological properties available during nanoparticle lubrication during high-temperature steel processing.

Acknowledgements

We are grateful to Mr. Joseph Abbott, Dr. Liang Hao, and Mr. Stuart Rodd for their assistance in the HR-AC experiments, and to Mr. D. Thi Ta and Mr. Linqing Pei for insightful discussions in MD simulation. The authors acknowledge use of facilities within the UOW Electron Microscopy Centre.

References

[1] B. Bhushan, Introduction to Tribology, John Wiley & Sons, Chichester, 2013.

[2] Z. Li, Q. Sun, M. Gao, Preparation of water-soluble magnetite nanocrystals from hydrated ferric salts in 2-pyrrolidone: mechanism leading to Fe_3O_4, Angew. Chem. Int. Ed. 44 (2005) 123–126.

[3] M. Krzyzanowski, J.H. Beynon, D.C. Farrugia, Oxide Scale Behavior in High Temperature Metal Processing, John Wiley & Sons, Weinheim, 2010.

[4] R.Y. Chen, W.Y.D. Yeun, Review of the high-temperature oxidation of iron and carbon steels in air or oxygen, Oxid. Met. 59 (2003) 433–468.

[5] D.B. Wei, J.X. Huang, A.W. Zhang, Z.Y. Jiang, A.K. Tieu, X. Shi, S.H. Jiao, X.Y. Qu, Study on the oxidation of stainless steels 304 and 304L in humid air and the friction during hot rolling, Wear 267 (2009) 1741–1745.

[6] R. Ghasemi, L. Elmquist, The relationship between flake graphite orientation, smearing effect, and closing tendency under abrasive wear conditions, Wear 317 (2014) 153–162.

[7] F.H. Stott, The role of oxidation in the wear of alloys, Tribol. Int. 31 (1998) 61–71.

[8] S. Spuzic, K.N. Strafford, C. Subramanian, G. Savage, Wear of hot rolling mill rolls: an overview, Wear 176 (1994) 261–271.

[9] G.W. Stachowiak, A.W. Batchelor, Corrosive and oxidative wear, in: Engineering Tribology 3rd ed., Elsevier, on-line, 2005. http://dx.doi.org/10.1016/B978-075067836-0/50014-6

[10] C. Vergne, C. Boher, R. Gras, C. Levaillant, Influence of oxides on friction in hot rolling: experimental investigations and tribological modelling, Wear, 260 (2006) 957–975.

[11] H.J. Li, Z.Y. Jiang, D.B. Wei, X.J. Gao, Influence of friction on surface asperity flattening process in cold uniaxial planar compression (CUPC), Tribol. Lett. 53 (2014) 383–393.

[12] H.J. Li, Z.Y. Jiang, D.B. Wei, Crystal plasticity finite modelling of 3D surface asperity flattening in uniaxial planar compression, Tribol. Lett. 46 (2012) 101–112.

[13] D.H. Buckley, Surface films and metallurgy related to lubrication and wear, Prog. Surf. Sci. 12 (1982) 1–153.

[14] X.L. Yu, Z.Y. Jiang, D.B. Wei, C.L. Zhou, Q.X. Huang, D.J. Yang, Tribological properties of magnetite precipitates from oxide scale in hot-rolled microalloyed steel, Wear 302 (2013) 1286–1294.

[15] O. Engler, V. Randle, Introduction to Texture Analysis: Macrotexture, Microtexture, and Orientation Mapping, 2nd ed., CRC press, Amsterdam, 2010.

[16] R.L. Higginson, B. Roebuck, E.J. Palmiere, Texture development in oxide scales on steel substrates, Scripta Mater. 47 (2002) 337–342.

[17] R. Lu, H. Zhang, Y. Mitsuya, K. Fukuzawa, S. Itoh, Influence of surface roughness and coating on the friction properties of nanometer-thick liquid lubricant films, Wear 319 (2014) 56–61.

[18] H. Wang, L. Yan, D. Gao, D. Liu, C. Wang, L. Sun, Y. Zhu, Tribological properties of superamphiphobic PPS/PTFE composite coating in the oilfield produced water, Wear (2014) 319 (2014) 62–68.

[19] D. Wang, X. Chen, M. Oeser, H. Stanjek, B. Steinauer, Study of micro-texture and skid resistance change of granite slabs during the polishing with the Aachen Polishing Machine, Wear 318 (2014) 1–11.

[20] E. Rabinowicz, Friction and Wear of Materials, 2nd ed., Wiley, New York, 1995.

[21] V. Randle, Microtexture Determination and Its Applications, 2nd ed., The Institute of Materials, London, 1992.

[22] H.-J. Bunge, Texture Analysis in Materials Science: Mathematical Methods, Butterworths, Berlin, 1982.

[23] J. Tang, A.K. Tieu, Z.Y. Jiang, Modelling of oxide scale surface roughness in hot metal forming, J. Mater. Process. Technol. 177 (2006) 126–129.

[24] G. Palumbo, K.T. Aust, E.M. Lehockey, U. Erb, P. Lin, On a more restrictive geometric criterion for “special” CSL grain boundaries, Scripta Mater. 38 (1998) 1685–1690.

[25] E.M. Lehockey, A.M. Brennenstuhl, I. Thompson, On the relationship between grain boundary connectivity, coincident site lattice boundaries, and intergranular stress corrosion cracking, Corros. Sci. 46 (2004) 2383–2404.

[26] V.Y. Gertsman, S.M. Bruemmer, Study of grain boundary character along intergranular stress corrosion crack paths in austenitic alloys, Acta Mater. 49 (2001) 1589–1598.

[27] S. Tsurekawa, S. Nakamichi, T. Watanabe, Correlation of grain boundary connectivity with grain boundary character distribution in austenitic stainless steel, Acta Mater. 54 (2006) 3617–3626.

[28] M. Shimada, H. Kokawa, Z.J. Wang, Y.S. Sato, I. Karibe, Optimization of grain boundary character distribution for intergranular corrosion resistant 304 stainless steel by twin-induced grain boundary engineering, Acta Mater. 50 (2002) 2331–2341.

[29] K.T. Aust, U. Erb, G. Palumbo, Interface control for resistance to intergranular cracking, Mater. Sci. Eng. A 176 (1994) 329–334.

[30] R. Cottam, V. Luzin, H. Moody, D. Edwards, A. Majumdar, Y.C. Wong, J. Wang, M. Brandt, The role of microstructural characteristics in the cavitation erosion behaviour of laser melted and laser processed Nickel–Aluminium Bronze, Wear 317 (2014) 56–63.

[31] T. Minoda, H. Yoshida, Effect of grain boundary characteristics on intergranular corrosion resistance of 6061 aluminium alloy extrusion, Metall. Mater. Trans. A 33 (2002) 2891–2898.

[32] B.K. Kim, J.A. Szpunar, Orientation imaging microscopy in research on high temperature oxidation, in: A.J. Schwartz (Ed.), Electron Backscatter Diffraction in Materials Science, Springer, New York, (2009), pp. 361–393.

[33] L. Suárez, P. Rodríguez-Calvillo, Y. Houbaert, N.F. Garza-Montes-de-Oca, R. Colás, Analysis of deformed oxide layers grown on steel, Oxid. Met. 75 (2011) 281–295.

[34] S. Birosca, D. Dingley, R.L. Higginson, Microstructural and microtextural characterization of oxide scale on steel using electron backscatter diffraction, J. Microsc. 213 (2004) 235–240.

[35] D.P. Burke, R.L. Higginson, Characterisation of multicomponent scales by electron back scattered diffraction (EBSD), Scripta Mater. 42 (2000) 277–281.

[36] C. Juricic, H. Pinto, D. Cardinali, M. Klaus, C. Genzel, A.R. Pyzalla, Effect of substrate grain size on the growth, texture and internal stresses of iron oxide scales forming at 450 °C, Oxid. Met. 73 (2010) 15–41.

[37] L.F. Morales, L.E. Lagoeiro, I. Endo, Crystallographic fabric development along a folded polycrystalline hematite, J. Struct. Geol. 30 (2008) 1218–1228.

[38] L.F. Morales, L.E. Lagoeiro, I. Endo, First results on the LPO-derived seismic properties of iron ores from the Quadrilátero Ferrífero region, southeastern Brazil, Tectonophysics 460 (2008) 21–33.

[39] Z.Y. Jiang, X.L. Yu, J.W. Zhao, C.L. Zhou, Q.X. Huang, G.Z. Luo, K.Z. Linghu, Tribological analysis of oxide scales during cooling process of rolled microalloyed steel, Adv. Mater. Res. 1017 (2014) 435–440.

[40] X.L. Yu, Z.Y. Jiang, J.W. Zhao, D.B. Wei, C.L. Zhou, Effect of cooling rate on oxidation behaviour of microalloyed steel, Appl. Mech. Mater. 395 (2013) 273–278.

[41] D.G. Brandon, The structure of high-angle grain boundaries, Acta Metall. 14 (1966) 1479–1484.

[42] X.L. Yu, Z.Y. Jiang, J.W. Zhao, D.B. Wei, C.L. Zhou, Q.X. Huang, Effect of a grain-refined microalloyed steel substrate on the formation mechanism of a tight oxide scale, Corros. Sci. 85 (2014) 115–125.

[43] J. Robertson, M.I. Manning, Limits to adherence of oxide scales, Mater. Sci. Tech. 6 (1990) 81–92.

[44] Y.N. Wang, J.C. Huang, Texture analysis in hexagonal materials, Mater. Chem. Phys. 81 (2003) 11–26.

[45] M.J. Philippe, F. Wagner, F.E. Mellab, C. Esling, J. Wegria, Modelling of texture evolution for materials of hexagonal symmetry–I. application to zinc alloys, Acta Metall. Mater. 42 (1994) 239–250.

[46] N.G. Condon, P.W. Murray, F.M. Leibsle, G. Thornton, A.R. Lennie, D.J. Vaughan, Fe_3O_4(111) termination of α-Fe_2O_3(0001), Surf. Sci. 310 (1994) L609–613.

[47] Y. Hu, V. Randle, An electron backscatter diffraction analysis of misorientation distributions in titanium alloys, Scripta Mater. 56 (2007) 1051–1054.

[48] J.G. Lenard, An examination of the coefficient of friction, in: J.G. Lenard (Ed.), Metal Forming Science and Practice: A State-of-the-Art Volume in Honour of Professor JA Schey's 80th Birthday, Elsevier, Oxford, (2002), pp.85–114.

[49] J.M. Alexander, R.C. Brewer, G.W. Rowe, Manufacturing Technology, Vol. 2: Engineering Processes, Ellis Horwood, Chichester, UK, 1993.

[50] P. Brito, H. Pinto, Ch. Genzel, M. Klaus, A. Kaysser-Pyzalla, Epitaxial stress and texture in thin oxide layers grown on Fe–Al alloys, Acta Mater. 60 (2012) 1230–1237.

[51] D.B. Wei, Z.Y. Jiang, J.T. Han, Modelling of the evolution of crack of nanoscale in iron, Computat. Mater. Sci. 69 (2013) 270–277.

[52] E.M. Lehockey, G. Palumbo, P. Lin, Grain boundary structure effects on cold work embrittlement of microalloyed steels, Scripta Mater. 39 (1998) 353–358.

[53]

Highlights

- Fe_3O_4 develops texture <001> parallel to the oxide growth.
- The deformed Fe_3O_4/α-Fe_2O_3 comprises a high proportion of low CSL boundaries.
- The decrease of coefficient of friction is due to changes in slip systems.
- Lubrication mechanism is proposed to improve tribological properties.

List of captions

Fig. 1 EBSD IPF orientation maps of the samples at the TRs and CRs of (a) 10%, 10 °C/s, (b) 13%, 23 °C/s, (c) 28%, 28 °C/s, a colour key for the (d) cubic symmetry of α-Fe, $Fe_{1-x}O$ and Fe_3O_4, and (e) hexagonal α-Fe_2O_3.

Fig. 2 Pole figures (PF) of Fe_3O_4 in oxide scale formed on the surface of the hot-rolled sample with a TR of 10% and a CR of 10 °C/s.

Fig. 3 Distributions of misorientation axes for grain boundaries in (a) Fe_3O_4, (b) α-Fe_2O_3, of the sample with a TR of 10% and a CR of 10 °C/s; distribution of grain boundary misorientation angels (c) from 2 to 62.8° for cubic Fe_3O_4, and (d) to 95° for hexagonal α-Fe_2O_3, of the samples with different TRs and CRs. Note the break in the vertical axis to emphasise the smaller peaks in comparison to the dominant peak less than 15°.

Fig. 4 Histogram plots of CSL boundary distribution for (a) Fe_3O_4 and (b) α-Fe_2O_3, of the samples with different TRs and CRs.

Fig. 5 The variation of the coefficient of friction and rolling force in different thickness reductions, microtexture and grain boundary characters in Fe_3O_4/Fe_2O_3 scale during hot rolling.

Fig. 6 Atomic configurations of nanoparticles flow along interface of tip of brittle crack. Note the size proportion of nanoparticles near the crack wall to emphasise the dominant crack tip.

Table 1 Chemical compositions of the microalloyed low carbon steel.